

# Hidden Data Embedding into Uninformative Subsets of Subband Image Projections

E. V. Bolgova<sup>a,\*</sup>, A. A. Chernomorets<sup>a</sup>, E. V. Petrova<sup>a</sup>, D. A. Chernomorets<sup>a</sup>, and D. V. Ursol<sup>a</sup>

<sup>a</sup>Belgorod State National Research University, Belgorod, 308015 Russia

\*e-mail: [bolgova\\_e@bsu.edu.ru](mailto:bolgova_e@bsu.edu.ru)

Received March 22, 2021; revised May 22, 2021; accepted July 2, 2021

**Abstract**—In this paper, we propose a method of subband hidden data embedding in images that can be applied to solve the actual problem of control over the distribution and use of images in information and telecommunication systems. The method is based on changing the values of subband projections of container images onto the eigenvectors of subband cosine-transformation matrices corresponding to a specified two-dimensional interval of spatial frequencies. A decision rule for choosing uninformative subsets of subband projections that can be used for hidden embedding is proposed. Comparative computational experiments were performed to estimate the distortions of container images during the data embedding based on the developed and other known methods. In some cases, the developed method of hidden subband embedding is shown to have an advantage in the secrecy of data embedding in images and allows them to be embedded without causing significant distortion of container images.

**Keywords:** hidden embedding, image, subband matrices, subband image projections, container-image distortion

**DOI:** 10.3103/S0147688222060016

## INTRODUCTION

In the process of exchanging information in the form of images in information and telecommunication networks, the problem of controlling their use arises. It is often associated with the need to respect copyright, for artistic photographs for example, as well as control over the use of data contained, for example, in images of the Earth's surface obtained as a result of aerospace monitoring, or in digital copies of various drawings, schematics, diagrams, etc.

One approach to organizing control over the distribution of images is the hidden embedding of identifying data into images that does not cause distortions, which can be detected visually or by appropriate processing. In this case, if necessary, the embedded data can be extracted without distortion [1–3].

In order to embed hidden data into images, in many cases, image processing is currently used based on the following sufficiently known methods:

- information hiding in the spatial domain, which is based on the change in the values of the image pixels themselves [1, 4]. One of the most commonly used methods of this group is the method of replacing the least significant bit of pixels (LSB). Many methods of this group are not resistant to external impacts that destroy embedded data, for example, to additive random noise;

- using the results of various orthogonal transformations, such as the Fourier transform, cosine transform, Haar transform, Hadamard transform, etc., to

hide data [4, 5]. These methods are based on making changes to the transform factors. Among the methods of this group, the method of the relative replacement of coefficients of the discrete cosine transform (DCT-Koch–Zhao method) became widespread [5, 6].

- spectrum extensions based on adding basic functions to the container image, which are built based on pseudo-random sequences with allowance for the bit values of the embedded data [4, 7].

Hidden embedding methods that use the results of orthogonal transformations, as well as spectrum expansions, are more resistant to destructive impacts compared to methods of hiding in the spatial domain. However, being quite universal, the known methods are developed from the standpoint of general requirements and do not completely take into account the specifics of the frequency properties of a specified image, which, in some cases, does not allow a high degree of secrecy of significant amounts of embedded information to be achieved.

In this paper, we propose to perform hidden embedding within the framework of subband analysis [3, 8, 9] of images based on the cosine transform, which adequately reflects the frequency properties of the images and is a real transform. The use of subband image analysis based on the mathematical apparatus of subband matrices [9–11] of cosine transform and their eigenvectors makes it possible to identify subband frequency components of images, such as image projections on eigenvectors of subband matrices of

cosine transform (subband projections) to varying degrees reflecting image information. Subband hidden embedding into a container image is based on changing its subband projections that do not contain essential information about the given image.

## 1. SUBBAND HIDDEN-EMBEDDING METHOD

The main provisions of the method of subband hidden embedding based on changing the subband projections of the image in the frame of cosine transformations are as follows.

Let us imagine a container image in which it is proposed to secretly embed data as matrix  $\Phi = (f_{ij})$ ,  $i = 1, 2, \dots, N_1$ ,  $j = 1, 2, \dots, N_2$  whose elements correspond to the pixel values of the image.

A domain of two-dimensional cosine transform is as follows:

$$D_\pi = \{(u, v) \mid 0 \leq u, v < \pi\}, \quad (1)$$

where  $u, v$  are the normalized spatial frequencies.

We represent as a union of specified number  $R_1 \times R_2$  of frequency intervals of spatial frequencies  $V_{r_1 r_2}$ ,  $r_1 = 1, 2, \dots, R_1$ ,  $r_2 = 1, 2, \dots, R_2$  of the following form:

$$V_{r_1 r_2} = D_{r_1} \cap C_{r_2}, \quad (2)$$

where subbands  $D_{r_1}$  and  $C_{r_2}$  of spatial frequencies in two-dimensional domain (1) have the form:

$$D_{r_1} = [u_{r_1,1}, u_{r_1,2}), \quad 0 \leq u_{r_1,1} < u_{r_1,2} < \pi, \quad r_1 = 1, 2, \dots, R_1, \quad (3)$$

$$C_{r_2} = [v_{r_2,1}, v_{r_2,2}), \quad 0 \leq v_{r_2,1} < v_{r_2,2} < \pi, \quad r_2 = 1, 2, \dots, R_2, \quad (4)$$

$$u_{r_1,1} = (r_1 - 1) \frac{\pi}{R_1}, \quad u_{r_1,2} = r_1 \frac{\pi}{R_1}, \quad v_{r_2,1} = (r_2 - 1) \frac{\pi}{R_2}, \quad (5)$$

$$v_{r_2,2} = r_2 \frac{\pi}{R_2}.$$

We choose the frequency interval that is used for hidden embedding. The choice of the interval can be based on various decision rules, for example, based on the analysis of the fraction values of the square of the image norm corresponding to various frequency intervals, where by the norm  $\|\Phi\|$  of image  $\Phi = (f_{ij})$ ,  $i = 1, 2, \dots, N_1$ ,  $j = 1, 2, \dots, N_2$  we mean the following value:

$$\|\Phi\| = \sqrt{\sum_{i=1}^{N_1} \sum_{j=1}^{N_2} f_{ij}^2}. \quad (6)$$

For specified frequency interval  $V_{r_1 r_2}$ , we construct subband cosine-transform matrices  $G_{r_1}$  and  $H_{r_2}$  [11,

12]. Matrix elements  $G_{r_1} = (g_{i_1 k_1}^{r_1})$ ,  $i_1, k_1 = 1, 2, \dots, N_1$  are determined by the following relations:

$$g_{in}^{r_1} = a_{in}^{r_1} + \tilde{g}_{in}^{r_1}, \quad (7)$$

$$a_{in}^{r_1} = \begin{cases} \frac{\sin(u_{r_1,2}(i-n)) - \sin(u_{r_1,1}(i-n))}{\pi(i-n)}, & i \neq n, \\ \frac{u_{r_1,2} - u_{r_1,1}}{\pi}, & i = n, \end{cases} \quad (8)$$

$$\tilde{g}_{in}^{r_1} = \frac{\sin(u_{r_1,2}(i+n-1)) - \sin(u_{r_1,1}(i+n-1))}{\pi(i+n-1)}. \quad (9)$$

Matrix elements  $H_{r_2} = (h_{i_2 k_2}^{r_2})$ ,  $i_2, k_2 = 1, 2, \dots, N_2$  are also calculated based on relations (7)–(9) by substituting frequency values  $v_{r_2,1}$  and  $v_{r_2,2}$  (5), respectively.

Subband matrices of form (7)–(9) are real, positive definite matrices. Therefore, subband cosine-transform matrices  $G_{r_1}$  and  $H_{r_2}$  have a complete set of eigenvectors  $\vec{q}_i^{r_1}$ ,  $i = 1, 2, \dots, N_1$ , and  $\vec{u}_k^{r_2}$ ,  $k = 1, 2, \dots, N_2$ .

Elements  $\gamma_{ik}^{r_1 r_2}$ ,  $i = 1, 2, \dots, N_1$ ,  $k = 1, 2, \dots, N_2$  of the form:

$$\gamma_{ik}^{r_1 r_2} = (\vec{q}_i^{r_1})^T \Phi \vec{u}_k^{r_2} \quad (10)$$

are called subband projections of image  $\Phi$  onto eigenvectors  $\vec{q}_i^{r_1}$ ,  $i = 1, 2, \dots, N_1$ , and  $\vec{u}_k^{r_2}$ ,  $k = 1, 2, \dots, N_2$  of subband cosine-transform matrices  $G_{r_1}$  and  $H_{r_2}$ .

The set of projections of form (10) of the  $\Phi$  image can be represented as a union of subsets  $\Psi_{s_1 s_2}$ ,  $s_1 = 1, 2, \dots, S_1$ ,  $s_2 = 1, 2, \dots, S_2$ :

$$\Psi_{s_1 s_2} = \{\gamma_{ik}^{r_1 r_2} \mid (s_1 - 1)N_1/S_1 + 1 \leq i \leq s_1 N_1/S_1, \quad (s_2 - 1)N_2/S_2 + 1 \leq k \leq s_2 N_2/S_2\}. \quad (11)$$

For each subset  $\Psi_{s_1 s_2}$ ,  $s_1 = 1, 2, \dots, S_1$ ,  $s_2 = 1, 2, \dots, S_2$  of form (11), we calculate the  $\delta_{s_1 s_2}$  value:

$$\delta_{s_1 s_2} = \frac{\sum_{i=(s_1-1)N_1/S_1+1}^{s_1 N_1/S_1} \sum_{k=(s_2-1)N_2/S_2+1}^{s_2 N_2/S_2} (\gamma_{ik}^{r_1 r_2})^2}{\sum_{i=1}^{N_1} \sum_{k=1}^{N_2} (\gamma_{ik}^{r_1 r_2})^2}. \quad (12)$$

It can be shown that the  $\delta_{s_1 s_2}$  value is a fraction of the square of the norm of the  $\Phi$  image matrix corresponding to the subband projections of subset  $\Psi_{s_1 s_2}$ .

For data embedding, it is proposed to choose subsets of subband projections that do not contain significant information about a given image (uninformative subsets of projections). In this case, subsets of projections containing essential information about a given image will be called informative. The significance of subset  $\Psi_{s_1 s_2}$  (11) of subband projections is proposed to

be estimated based on  $\delta_{s_1 s_2}$  value (12) of the fraction of the square of the image norm.

We formulate a decision rule for choosing informative and uninformative subband image projections as follows. We set the  $T_p$  threshold value, the level of significance of subsets of projections:

$$0 < T_p \leq 1 \quad (13)$$

corresponding to some fraction of the square of the norm of the container image.

We consider the ordered set  $W^\Psi = \{w_k^\Psi\}$ ,  $k = 1, 2, \dots, S_1 S_2$  whose elements are  $\delta_{s_1 s_2}$  values (12),  $s_1 = 1, 2, \dots, S_1$ ,  $s_2 = 1, 2, \dots, S_2$  in descending order.

We calculate the value of the ordinal number of elements  $l_{T_p}$  in set  $W^\Psi$ ,  $1 \leq l_{T_p} \leq S_1 S_2$ , for which the following conditions are satisfied:

$$\sum_{k=1}^{l_{T_p}} w_k^\Psi \leq T_p \quad \text{and} \quad \sum_{k=1}^{l_{T_p}+1} w_k^\Psi > T_p. \quad (14)$$

We create a set of indices  $Z_{T_p} = \{(s_1, s_2)\}$  of subset  $\Psi_{s_1 s_2}$  corresponding to the first  $l_{T_p}$  elements of ordered set  $W^\Psi$ .

The subsets of subband projections included in set  $Z_{T_p}$  are informative for significance level  $T_p$  while the remaining subsets are uninformative.

We consider hidden subband data embedding into a specified uninformative subset of subband projections of container image  $\Phi = (f_{ij})$ ,  $i = 1, 2, \dots, N_1$ ,  $j = 1, 2, \dots, N_2$ .

To implement hidden embedding, we represent the hidden information as a sequence of bits:  $B = (b_m)$ ,  $m = 1, 2, \dots, N_B$ .

We consider the embedding of single bit  $b_m$  using uninformative subband projections of projections  $\gamma_{ik}^{n_2}$  and  $\gamma_{i,k+1}^{n_2}$  of form (10) of container image  $\Phi$  that are formed by corresponding eigenvectors  $\vec{q}_i^{n_1}$ ,  $\vec{u}_k^{n_2}$  and  $\vec{q}_i^{n_1}$ ,  $\vec{u}_{k+1}^{n_2}$ .

If embedded bit  $b_m$  is equal to zero, then we change the corresponding values of projections  $\gamma_{ik}^{n_2}$  and  $\gamma_{i,k+1}^{n_2}$  in such a way that the following inequality for the changed values of  $\tilde{\gamma}_{ik}^{n_2}$  and  $\tilde{\gamma}_{i,k+1}^{n_2}$  is fulfilled:

$$\left| \tilde{\gamma}_{ik}^{n_2} \right| \geq \left| \tilde{\gamma}_{i,k+1}^{n_2} \right| + T_\gamma^{s_1 s_2}, \quad (15)$$

where  $T_\gamma^{s_1 s_2}$  is the threshold value of the relative difference of the changed projections, otherwise ( $b_m = 1$ ) to satisfy the inequality:

$$\left| \tilde{\gamma}_{ik}^{n_2} \right| \leq \left| \tilde{\gamma}_{i,k+1}^{n_2} \right| - T_\gamma^{s_1 s_2}. \quad (16)$$

The direct embedding of a data bit into container image  $\Phi$  is carried out based on the relation:

$$\begin{aligned} \tilde{\Phi} = \Phi &+ (\tilde{\gamma}_{ik}^{n_2} - \gamma_{ik}^{n_2}) \vec{q}_i^{n_1} (\vec{u}_k^{n_2})^T \\ &+ (\tilde{\gamma}_{i,k+1}^{n_2} - \gamma_{i,k+1}^{n_2}) \vec{q}_i^{n_1} (\vec{u}_{k+1}^{n_2})^T, \end{aligned} \quad (17)$$

where  $\tilde{\Phi}$  is the container image containing embedded information.

The value of a single bit of data from container image  $\tilde{\Phi}$  that is embedded and hidden using pairs of eigenvectors  $\vec{q}_i^{n_1}$ ,  $\vec{u}_k^{n_2}$  and  $\vec{q}_i^{n_1}$ ,  $\vec{u}_{k+1}^{n_2}$  is retrieved as follows. We calculate projections  $\tilde{\gamma}_{ik}^{n_2}$  and  $\tilde{\gamma}_{i,k+1}^{n_2}$  of form (10) of image  $\tilde{\Phi}$  onto the selected pairs of eigenvectors  $\vec{q}_i^{n_1}$ ,  $\vec{u}_k^{n_2}$  and  $\vec{q}_i^{n_1}$ ,  $\vec{u}_{k+1}^{n_2}$ .

Then, to determine the value of retrieved information bit  $\tilde{b}_m$ , the following conditions are used:

$$\tilde{b}_m = \begin{cases} 0, & \left| \tilde{\gamma}_{ik}^{n_2} \right| \geq \left| \tilde{\gamma}_{i,k+1}^{n_2} \right|, \\ 1, & \text{otherwise.} \end{cases} \quad (18)$$

To embed simultaneously information in other uninformative subband projections, it necessary to follow the same steps as above.

The  $T_\gamma^{s_1 s_2}$  threshold value used in (15) and (16) is given by:

$$T_\gamma^{s_1 s_2} = t_\gamma \gamma_{cp}^{s_1 s_2}, \quad (19)$$

where  $t_\gamma$  is the embedding factor that makes it possible to refine interactively the  $T_\gamma^{n_2}$  threshold value,

$$t_\gamma \geq 0, \quad (20)$$

$\gamma_{cp}^{s_1 s_2}$  is a characteristic of the projection values included in selected subset  $\Psi_{s_1 s_2}$ ,

$$\gamma_{cp}^{s_1 s_2} = \sqrt{\frac{\sum_{i=(s_1-1)N_1/S_1+1}^{s_1 N_1/S_1} \sum_{k=(s_2-1)N_2/S_2+1}^{s_2 N_2/S_2} (\gamma_{ik}^{n_2})^2}{\left( \frac{N_1 N_2}{S_1 S_2} \right)}}. \quad (21)$$

In the event that, when performing hidden subband data embedding in the container image, the requirements for the results of embedding, for example, according to the magnitude of the distortion of the container image or by the stability of the embedded data to additive random noise affecting the image-container are not met, then threshold  $T_p$  value (13), which determines the significance level of projection subsets, and embedding factor  $t_\gamma$  (20), is specified, applying, for example, production knowledge about the properties of the frequency components of images.

We performed computational experiments to test the efficiency of the developed method.

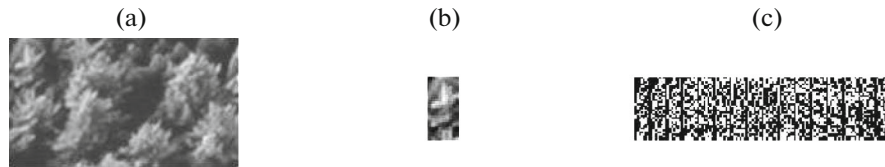


**Fig. 1.** Representation of embedded data: (a) initial image, (b) embedded fragment, and (c) binary representation of the embedded data.

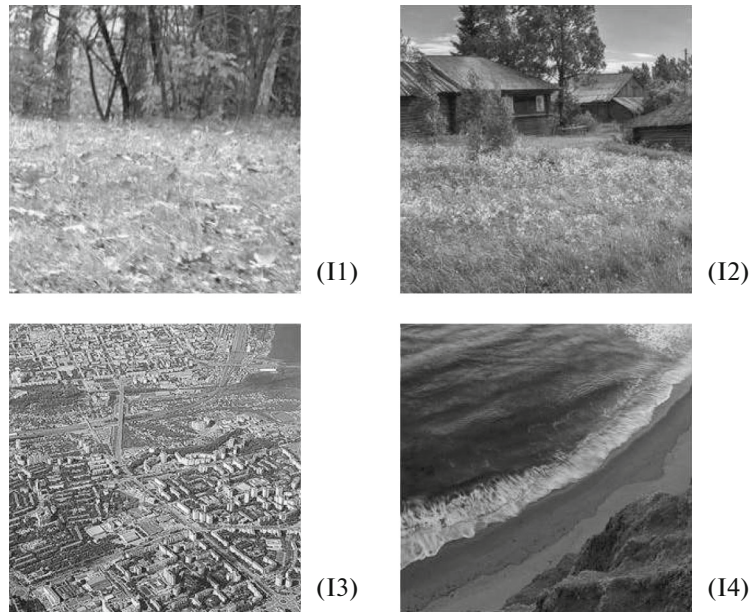


**Fig. 2.** Container images.

## 2. COMPUTATIONAL EXPERIMENTS

The secrecy of the embedding results (container image distortions) obtained using the developed method is estimated based on calculating the standard deviation of container image  $\tilde{\Phi} = (\tilde{f}_{ij})$ ,  $i = 1, 2, \dots, N_1$ ,  $j = 1, 2, \dots, N_2$  with embedded data relative to initial image  $\Phi = (f_{ij})$ ,  $i = 1, 2, \dots, N_1$ ,  $j = 1, 2, \dots, N_2$ :

$$\sigma = \sqrt{\frac{\sum_{i=1}^{N_1} \sum_{j=1}^{N_2} (\tilde{f}_{ij} - f_{ij})^2}{\sum_{i=1}^{N_1} \sum_{j=1}^{N_2} f_{ij}^2}}. \quad (22)$$

To evaluate the container image distortions, computational experiments on the embedding of 4096 bits of data generated based on a fragment with a dimension of  $32 \times 16$  pixels (Fig. 1a) were performed. The amount of embedded data is limited to 4096 bits, as the known methods used in computational experiments do not allow more bits to be hidden and embedded (for example, when using the Koch–Zhao method [4–6]).

Embedding in images I1, I2, I3, and I4 (in gray-scale) was performed; dimensions are  $512 \times 512$  pixels (Fig. 2).

The images used in the computational experiments were obtained from open sources on the Internet. One of the distinguishing features of the analyzed images is the presence of large or small details, as well as the presence or absence of image areas with smooth brightness transitions.

In hidden embedding based on the developed method, the following embedding factors were used:  $t_\gamma = \{0.08, 0.1, 0.5, 0.8, 1, 1.5, 2, 2.5\}$ , as well as the threshold values of the fraction of the squared norm of the image matrix:  $T_p = \{0.997, 0.998, 0.9985, 0.999, 0.9995\}$ , which made it possible to obtain various distortions of container images.

In computational experiments, the definition domain of the cosine transform was divided into  $16 \times 16$  frequency domains. To construct subband projections of images onto the eigenvectors of subband matrices, we used subband matrices  $H_{16}$  and  $G_{16}$  of form (7)–(9), corresponding to the frequency interval, the boundaries (5) of which have the values:

$$u_{16,1} = \frac{15}{16}\pi, \quad u_{16,2} = \pi, \quad v_{16,1} = \frac{15}{16}\pi, \quad v_{16,2} = \pi.$$

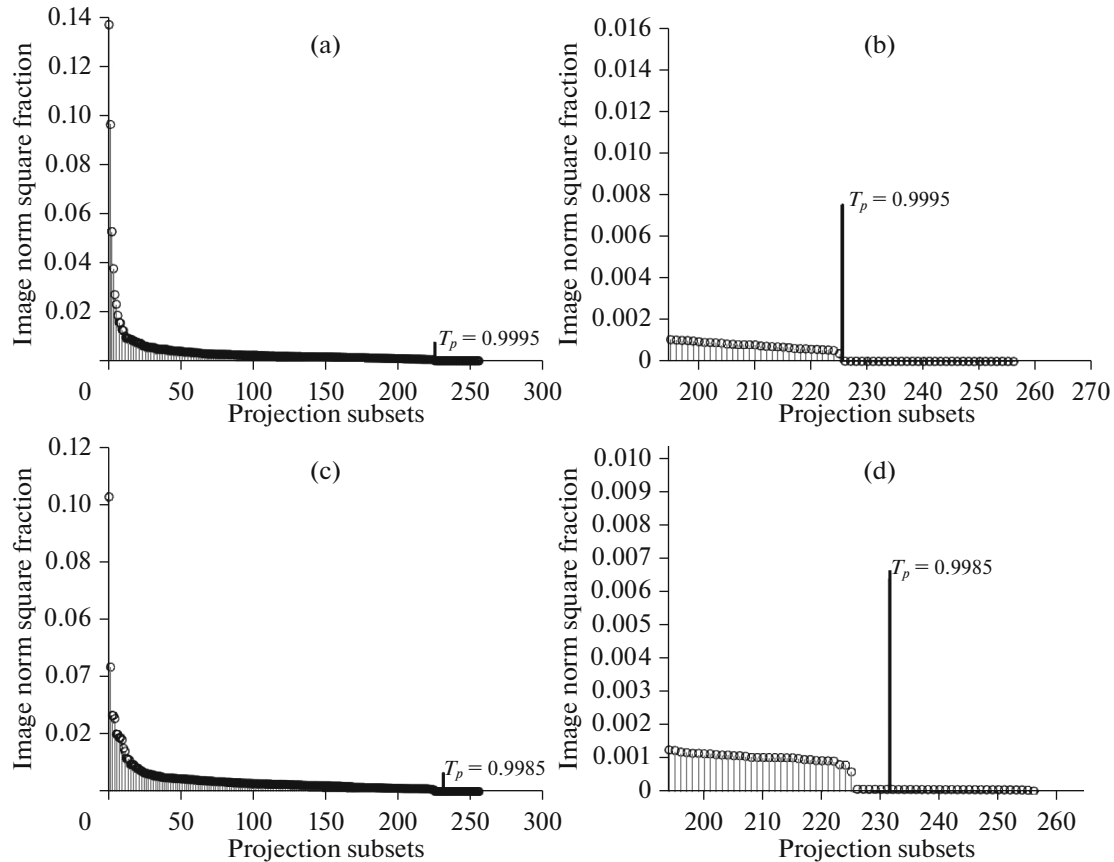


**Fig. 3.** Ordered values of the fraction of the squared norm of images I1 and I2 that correspond to subsets of subband projections: (a, b) for image I1, and (c, d) for image I2.

The set of obtained subband projections was divided into  $16 \times 16$  subsets of form (11).

To select informative and uninformative subsets of subband projections recommended for embedding, sequences of fraction values (12) of the square of the image norm corresponding to subsets of subband projections were constructed.

Figures 3 and 4 show graphs of the ordered fraction values of the norm square of images I1–I4, corresponding to subsets of subband projections. The graphs also show various  $T_p$  threshold values, based on which the subsets of projections are divided into informative and uninformative classes in the developed method. Various values of  $T_p$  are selected to demonstrate the difference in the subband properties of the images shown in the figures. Figures 3b, 3d, 4b, and 4d show enlarged fragments of the graphs presented in Figs. 3a, 3c, 4a, and 4c in order to increase the information content.

Figures 3 and 4 show the division of subsets of subband projections into classes in accordance with the specified  $T_p$  threshold value ( $T_p = \{0.9995, 0.9985, 0.998, 0.999\}$  for images I1–I4, respectively); taking

this into account makes it possible to obtain minor distortions of the container image at hidden embedding based on the developed method.

Informative (grey cells) and uninformative (white cells) subsets of subband projections of I1–I4 images corresponding to the threshold values indicated in Figs. 3 and 4 are schematically marked in Fig. 5.

The data shown in Figs. 3–5 illustrate the subband properties of images, taking into account which makes it possible to obtain a high degree of hiddenness of data embedding based on the developed method of adaptive subband hidden embedding.

Tables 1–4 show the results of hiddenness evaluation for cases in which the embedded data were retrieved (recovered) without distortion. Note that in the computational experiments, the distortion of embedded data is associated with the accuracy of their representation when performing the required image transformations.

Tables 1 and 2 show the values of distortions (standard deviation (22)) of I1–I4 container images obtained as a result of hidden embedding of 4096 bits of data based on the developed method.

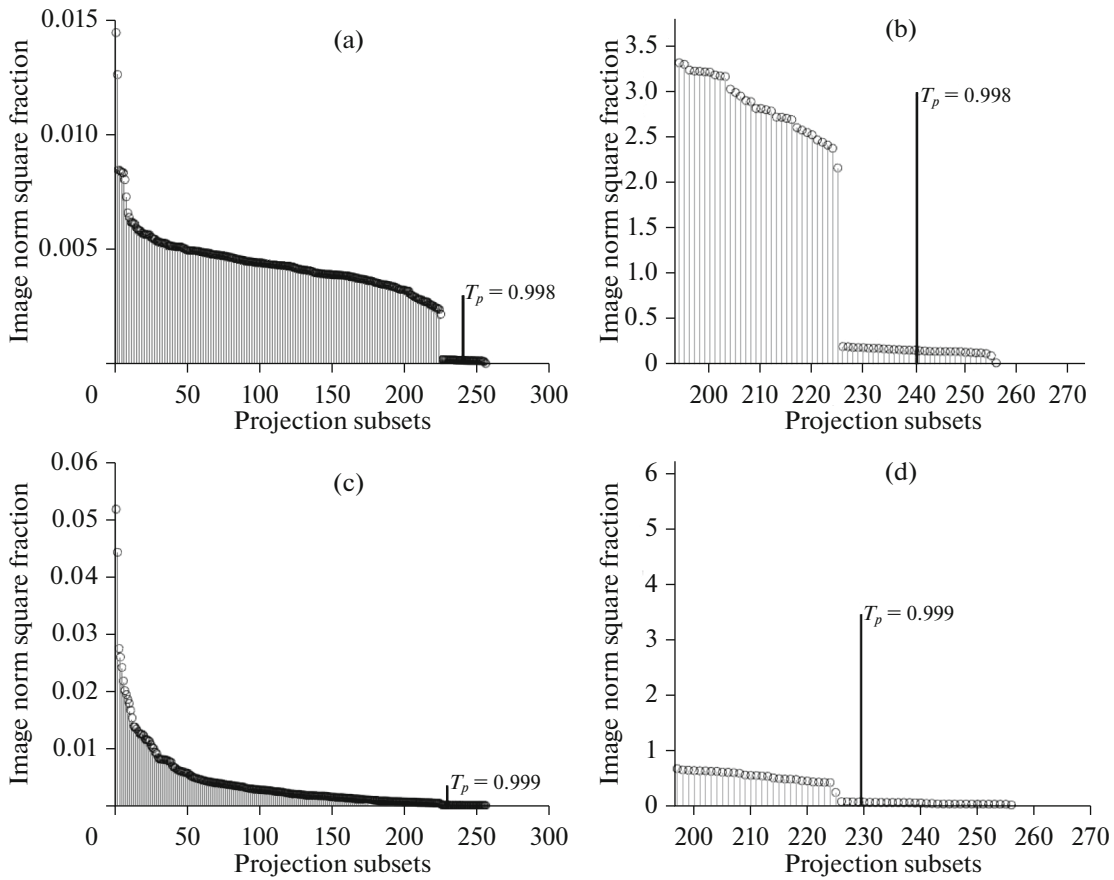


**Fig. 4.** Ordered values of the fraction of the squared norm of images I3 and I4 that correspond to subsets of subband projections: (a, b) for image I3, and (c, d) for image I4.

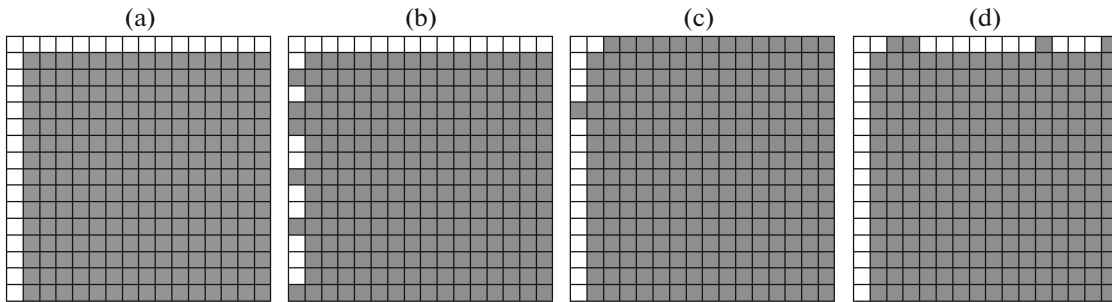


**Fig. 5.** Partitioning into informative and uninformative classes of subsets of subband image projections: (a) for image I1 at  $T_p = 0.9995$ , (b) for image I2 at  $T_p = 0.9985$ , (c) for image I3 at  $T_p = 0.998$ , and (d) for image I4 at  $T_p = 0.999$ .

Table 1 shows the values of the root-mean-square deviation obtained by hidden embedding subband projections into uninformative subsets, constructed for various  $T_p$  threshold values (13) of the fraction of the squared norm of the corresponding image. There also indicated the value of factor  $t_\gamma$  (20), which was used during embedding in the corresponding image.

The data in Table 1 show that an increase in the  $T_p$  threshold value makes it possible to increase the hiddenness of embedding (in this case, the value of the standard deviation decreases).

Table 2 shows the values of the standard deviation of container images I1–I4, obtained as a result of hidden embedding at various values of embedding factor  $t_\gamma$ .

**Table 1.** Distortion (standard deviation) of container images depending on the  $T_p$  threshold value

| Threshold $T_p$ | Image I1, $t_\gamma = 2$ | Image I2, $t_\gamma = 0.5$ | Image I3, $t_\gamma = 0.08$ | Image I4, $t_\gamma = 0.8$ |
|-----------------|--------------------------|----------------------------|-----------------------------|----------------------------|
| 0.997           | 0.12                     | 0.038                      | 0.029                       | 0.04                       |
| 0.998           | 0.091                    | 0.01                       | 0.027                       | 0.03                       |
| 0.9985          | 0.07                     | 0.009                      | 0.025                       | 0.017                      |
| 0.999           | 0.041                    | 0.0088                     | —                           | 0.009                      |
| 0.9995          | 0.0047                   | 0.008                      | —                           | 0.008                      |

**Table 2.** Distortion (standard deviation) of container images depending on embedding factor  $t_\gamma$ 

| Coefficient $t_\gamma$ | Image I1, $T_p = 0.9995$ | Image I2, $T_p = 0.998$ | Image I3, $T_p = 0.998$ | Image I4, $T_p = 0.999$ |
|------------------------|--------------------------|-------------------------|-------------------------|-------------------------|
| 2.5                    | 0.005                    | 0.022                   | 0.11                    | 0.017                   |
| 2                      | 0.0047                   | 0.019                   | 0.058                   | 0.015                   |
| 1.5                    | —                        | 0.016                   | 0.048                   | 0.012                   |
| 1                      | —                        | 0.013                   | 0.039                   | 0.01                    |
| 0.8                    | —                        | 0.012                   | 0.036                   | 0.009                   |
| 0.5                    | —                        | 0.01                    | 0.032                   | —                       |
| 0.1                    | —                        | —                       | 0.027                   | —                       |
| 0.08                   | —                        | —                       | 0.027                   | —                       |

**Table 3.** Distortion (root-mean-square deviation) of container images when applying the Koch–Zhao method

| Threshold value $P$ | Image I1 | Image I2 | Image I3 | Image I4 |
|---------------------|----------|----------|----------|----------|
| 25                  | 0.039    | 0.035    | 0.095    | 0.078    |
| 20                  | 0.037    | 0.032    | 0.092    | 0.069    |
| 15                  | 0.033    | 0.029    | 0.09     | 0.063    |
| 10                  | 0.033    | 0.026    | 0.088    | 0.059    |
| 5                   | 0.029    | 0.021    | 0.085    | 0.055    |
| 4                   | 0.029    | 0.021    | 0.085    | 0.055    |

**Table 4.** Distortion (root mean square deviation) of container images when applying the spectrum expansion method

| Coefficient $K$   | Image I1 | Image I2 | Image I3 | Image I4 |
|---|----------|----------|----------|----------|
| Initial version of the method                                   |          |          |          |          |
| Value of the $K$ coefficient is calculated during embedding     | 0.015    | 0.026    | 0.041    | 0.025    |
| Modified version of the method.<br>$K$ coefficient value is set |          |          |          |          |
| 5   | 0.037    | 0.043    | 0.041    | 0.062    |
| 4   | 0.029    | 0.034    | 0.033    | 0.049    |
| 3   | 0.022    | 0.026    | —        | 0.037    |
| 2   | 0.015    | —        | —        | 0.025    |
| 1   | 0.007    | —        | —        | —        |

For each image, a  $T_p$  threshold value is also indicated, according to which uninformative subsets of subband projections were selected for embedding.

The data in Table 2 show that an increase in the hiddenness of the embedding results when applying the developed method can be obtained by reducing embedding factor  $t_\gamma$ . They also demonstrate that the application of the developed method makes it possible to obtain rather low distortions of container images as a result of data embedding.

The following are the results of computational experiments that make it possible to perform a comparative estimate of the hiddenness of the results of embedding using known methods, such as the relative change in the DCT coefficients (the Koch–Zhao method) [5, 6] and spectrum expansion [4, 7].

Table 3 shows the values of the standard deviation of container images I1–I4 at hidden data embedding of 4096 bits using the Koch–Zhao method. The embedding results were obtained at the various  $P$  threshold values [4] of the relative change in the DCT coefficients.

Table 4 shows the values of the standard deviation of container images I1–I4 obtained as a result of hidden data embedding of 4096 bits using the spectrum expansion method. The embedding results obtained at various coefficients  $K$  [4], by which the pseudo-random sequences used in this method are multiplied, are given.

The data given in Tables 1–4 show that the developed method of subband hidden embedding makes it

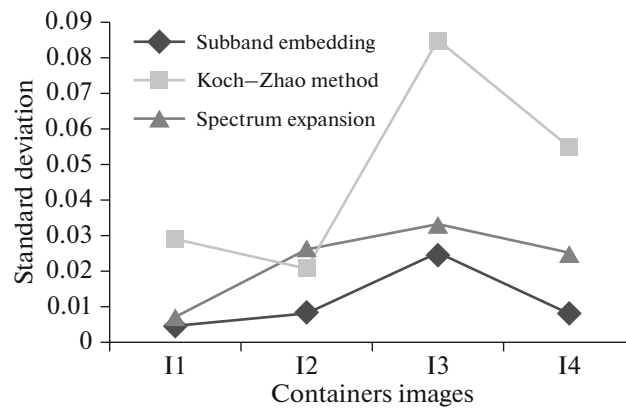


Fig. 6. Comparative evaluation of container image distortions.

possible, in some cases, to obtain lower values of distortion (standard deviation) of container images compared to the Koch–Zhao and spectrum extension methods.

In order to increase the visibility of estimating the hiddenness of the hiddenness results when using the developed and other methods, Fig. 6 shows the values corresponding to the lowest distortions of container images obtained during computational experiments. The results shown in Tables 1–4 and Fig. 6 illustrate the advantages of the developed method of subband hidden embedding in the hiddenness of data embedding in images compared to such well-known methods as the Koch–Zhao method and the spectrum expansion method. The experiments also showed that the application of the developed method makes it possible to obtain minor distortions of container images during data embedding.

## CONCLUSIONS

Based on the concept of subband projections of an image onto eigenvectors of subband cosine-transform matrices, a method of subband hidden embedding of data into images, which consists in changing the values of uninformative subband projections depending on the information being embedded, was developed. A decision rule for choosing uninformative subsets of subband projections recommended for hidden embedding is proposed.

The results of the computational experiments showed the operability of the developed method of subband hidden embedding within the framework of the cosine transform and demonstrated the advantages of the developed method from the standpoint of the hiddenness of data embedding. The developed method is shown to make it possible to obtain smaller distortions of container images during data embedding in comparison with the known methods of relative replacement of DCT coefficients and spectrum expansion.

The method and the decision rule proposed here can be used in the development of an intelligent information system for the hidden embedding of information into images, which makes it possible to achieve a high degree of hiddenness of data embedding based on making decisions about the rational values of the applied embedding parameters.

## FUNDING

The work was supported by the Russian Foundation for Basic Research, project no. 19-07-00657.

## CONFLICT OF INTEREST

The authors declare that they have no conflicts of interest.

## REFERENCES

- Gribunin, V.G., Okov, I.N., and Turintsev, I.V., *Tsifrovaya steganografiya* (Digital Steganography), Moscow: Solon-Press, 2016.
- Agranovskii, A.V., *Steganografiya, tsifrovye vodyanye znaki i steganoanaliz* (Steganography, Digital Watermarks, and and Stegananalysis), Moscow: Vuzovskaya Kniga, 2009.
- Zhilyakov, E.G., Chernomorets, A.A., Bolgova, E.V., and Gahova, N.N., Investigation of the steganography stability in images, *Nauchn. Ved. Belgorod. Gos. Univ. Ser.: Ekon. Inf.*, 2014, no. 1, pp. 168–174.
- Konakhovich, G.F. and Puzyrenko, A.Yu., *Komp'yuternaya steganografiya. Teoriya i praktika* (Computer Steganography: Theory and Practice), Kiev: MK-Press, 2006.
- Koch, E. and Zhao, J., Towards robust and hidden image copyright labeling, *Proc. 1995 IEEE Workshop on Nonlinear Signal and Image Processing*, Neos Marmaras, Greece, 1995, IEEE, 1995.
- Chernomorets, A.A. and Bolgova, E.V., About the accuracy of steganographic embedding in the image using method of relative replacement of DCT coefficients, *Inf. Sist. Tekhnol.*, 2012, no. 6, pp. 125–131.

7. Smith, J.R. and Comiskey, B.O., *Modulation and information hiding in images, Information Hiding*, Anderson, R., Ed., Lecture Notes in Computer Science, vol. 1174, Berlin: Springer, 1996, pp. 207–226.  
[https://doi.org/10.1007/3-540-61996-8\\_42](https://doi.org/10.1007/3-540-61996-8_42)
8. Zhilyakov, E.G., Chernomorets, A.A., Belov, A.S., and Bolgova, E.V., On subband properties of images, *Nauchn. Ved. Belgorod. Gos. Univ. Ser.: Ekon. Inf.*, 2013, no. 7, pp. 175–182.
9. Bolgova, E.V., Chernomorets, A.A., and Chernomorets, D.A., Subband image analysis in the cosine transform definition domain, *Inf. Sist. Tekhnol.*, 2019, no. 6, pp. 5–11.
10. Chernomorets, D.A., Bolgova, E.V., Chernomorets, A.A., and Barsuk, A.A., Images presentation based on subband cosine transform matrix eigenvectors basis, *Nauchn. Rezul'tat. Inf. Tekhnol.*, 2019, vol. 4, no. 1, pp. 3–8.  
<https://doi.org/10.18413/2518-1092-2019-4-1-0-1>
11. Zhilyakov, E.G., Chernomorets, A.A., Bolgova, E.V., Petina, M.A., and Kovalenko, A.N., The properties and application of the cosine transform subband matrices, *J. Adv. Res. Dynamical Control Syst.*, 2020, vol. 15, no. 5, pp. 1302–1313.  
<https://doi.org/10.5373/JARDCS/V12SP5/20201890>
12. Chernomorets, A.A., Bolgova, E.V., and Chernomorets, D.A., On quasi-subband matrices of cosine transform, *Nauchn. Rezul'tat. Inf. Tekhnol.*, 2019, vol. 4, no. 3, pp. 11–19.  
<https://doi.org/10.18413/2518-1092-2019-4-3-0-2>

*Translated by A. Ivanov*